Supplementary material for

Sources of ultrafine particles at a typical rural Midland site in Switzerland

by Dada et al.

This document contains 1 supplementary table and 26 supplementary figures.

Table S 1 Summary of variables measured in Payerne during our measurement campaign.

Parameter	Instrument	Time resolution	Measurement period
Campaign instrumentation			
Particle number size distribution (2.5 – 14.5 nm)	NAIS	5 min	09 October 2020 to 31 July 2021
Particle number size distribution (10 – 487 nm nm)	SMPS 3034, CPC 3022A	3 min	01 July 2020 to July 31 2021
Positively charged particles (0.8 – 40 nm)	NAIS	5 min	09 October 2020 to 31 July 2021
Negatively charged particles (0.8 – 40 nm)	NAIS	5 min	09 October 2020 to 31 July 2021
Non-volatile particle number size distribution (6 – 110 nm)	SMPS 3938, CPC 3775	1 min	19 December 2020 to 03 March 2021
Continuous monitoring (ongoing)			
Equivalent black carbon	Aethalometer AE-31	1 hour	01 July 2020 to July 31 2021
Trace gases	Thermo Scientific 49i (O_3), Teledyne API T500U (NO_2) Thermo Scientific 43i TLE (SO_2)	1 hour	
Ammonia (NH_3)	Picarro G2103	10 min	
Meteorological parameters*	SwissMetNet**	10 min	

**Meteorological parameters include temperature, global radiation, RH, precipitation, wind direction and wind speed.*

***https://www.meteoswiss.admin.ch/weather/measurement-systems/land-based-stations/automatic-measurement-network.html, last access 02.10.2024*

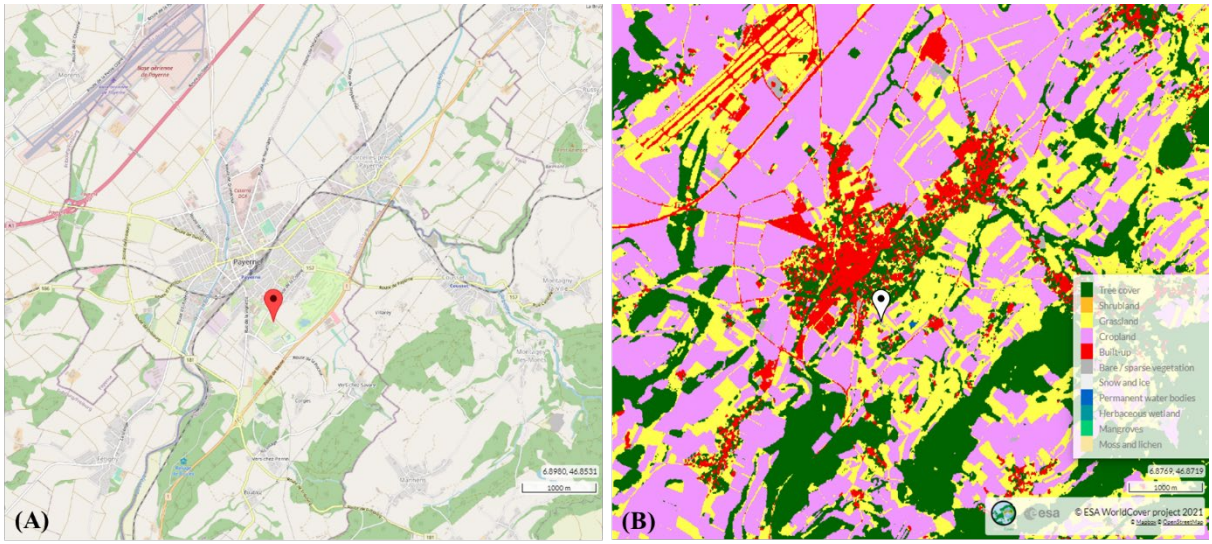

Figure S 1 (A) Location and (B) land use information of Payerne measurement station marked with red and white pins respectively. Maps are extracted from from ESA WorldCover ©.

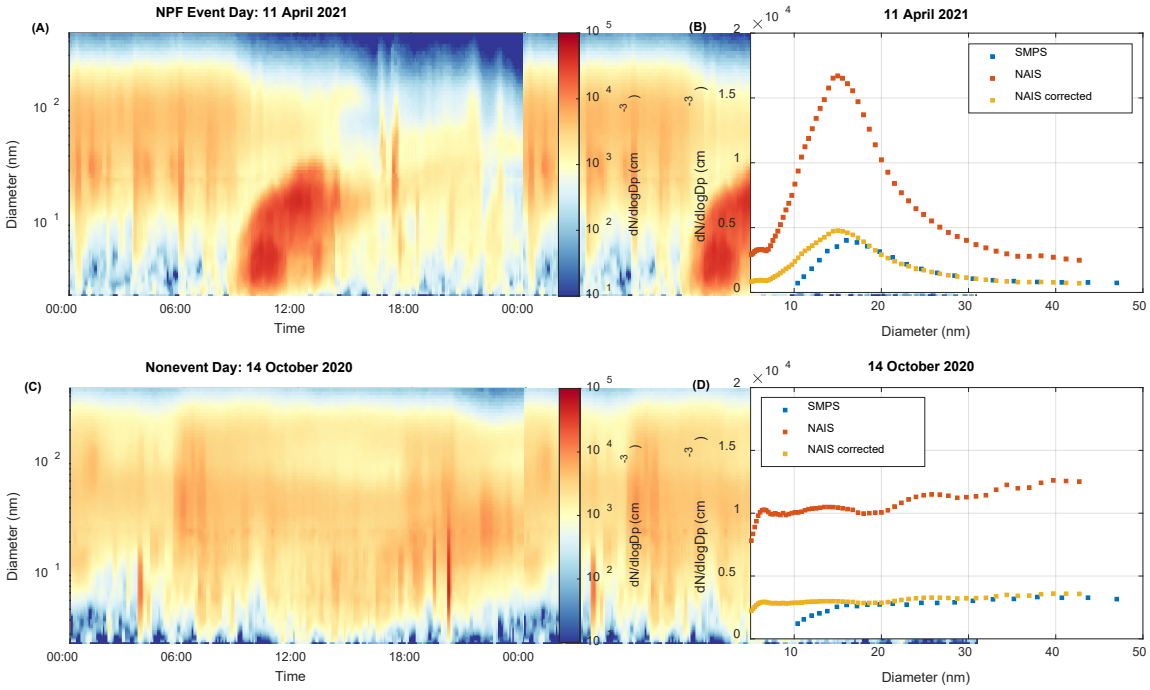

Figure S 2 Examples of combined particle number size distribution using SMPS and corrected NAIS data on (A) an NPF event day and a (C) nonevent day and the corresponding one hour (here at 15:00 chosen randomly) average number concentration as a function of diameter shown in (B) and (D), respectively. A 3.5 correction factor was applied to the NAIS concentrations.

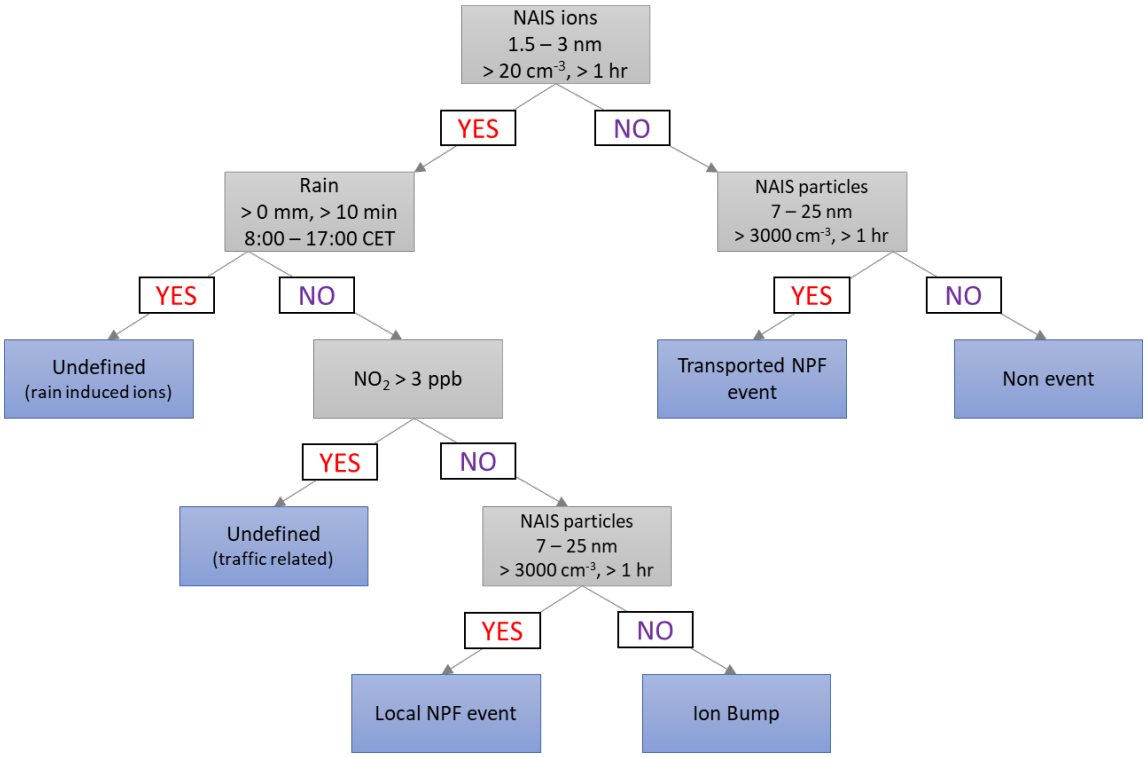

Figure S 3 Flowchart for the event classification adapted for Payerne based on Dada et al. (2018).

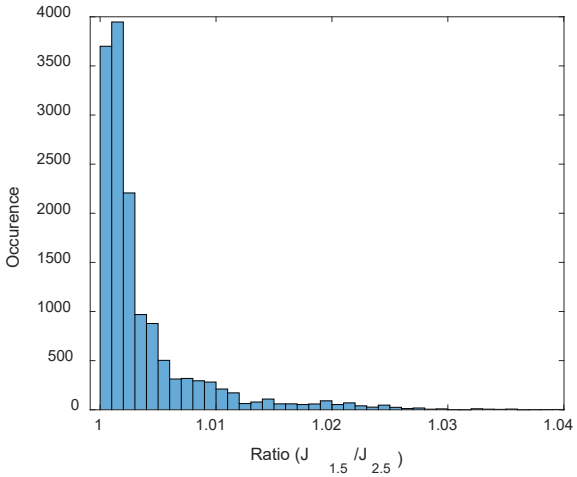

Figure S 4 Histogram of the ratio between calculated $J_{1.5}$ using the Kerminen and Kulmala (2002) equation and $J_{2.5}$ calculated from measured size distributions.

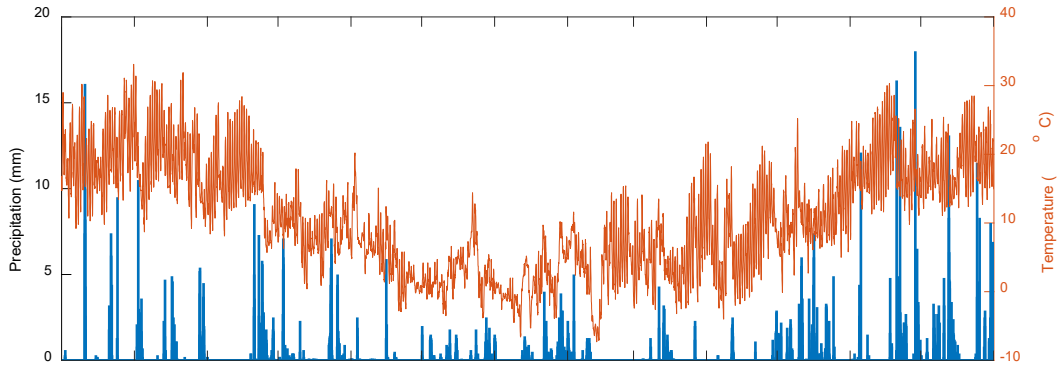

Figure S 5 Time series (hourly data) of precipitation (blue) and temperature (orange) variations in Payerne during our measurement period July 2020 – July 2021. Tick labels refer to the beginning of every month.

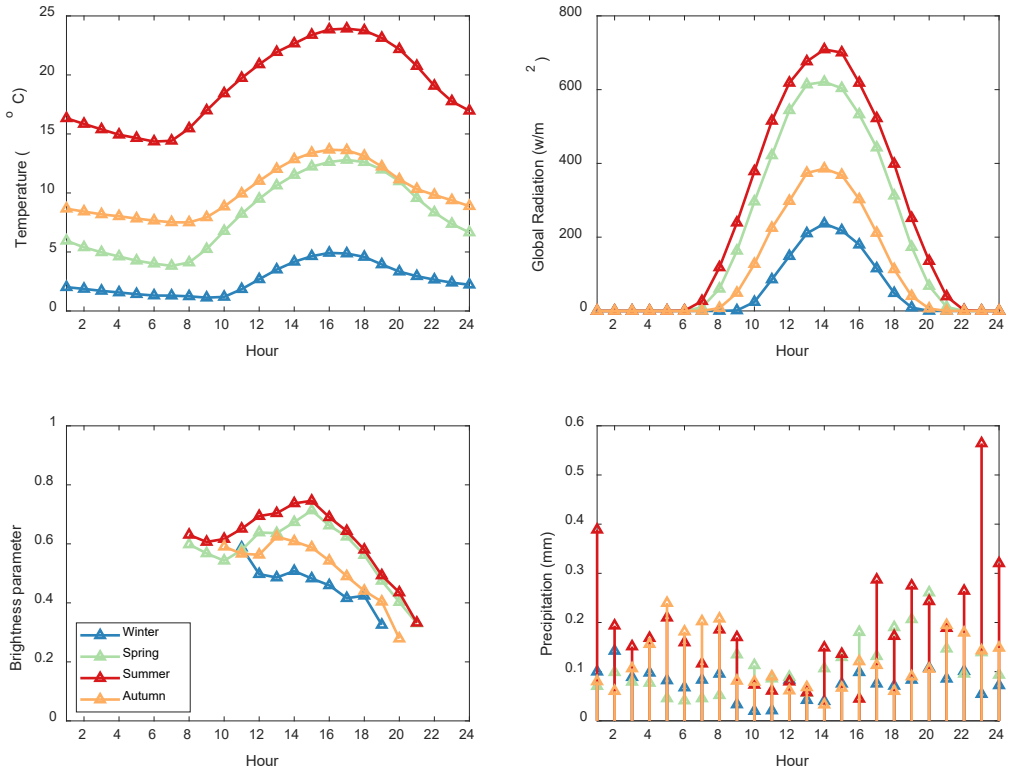

Figure S 6 Seasonal diurnal averages of meteorological parameters in Payerne.

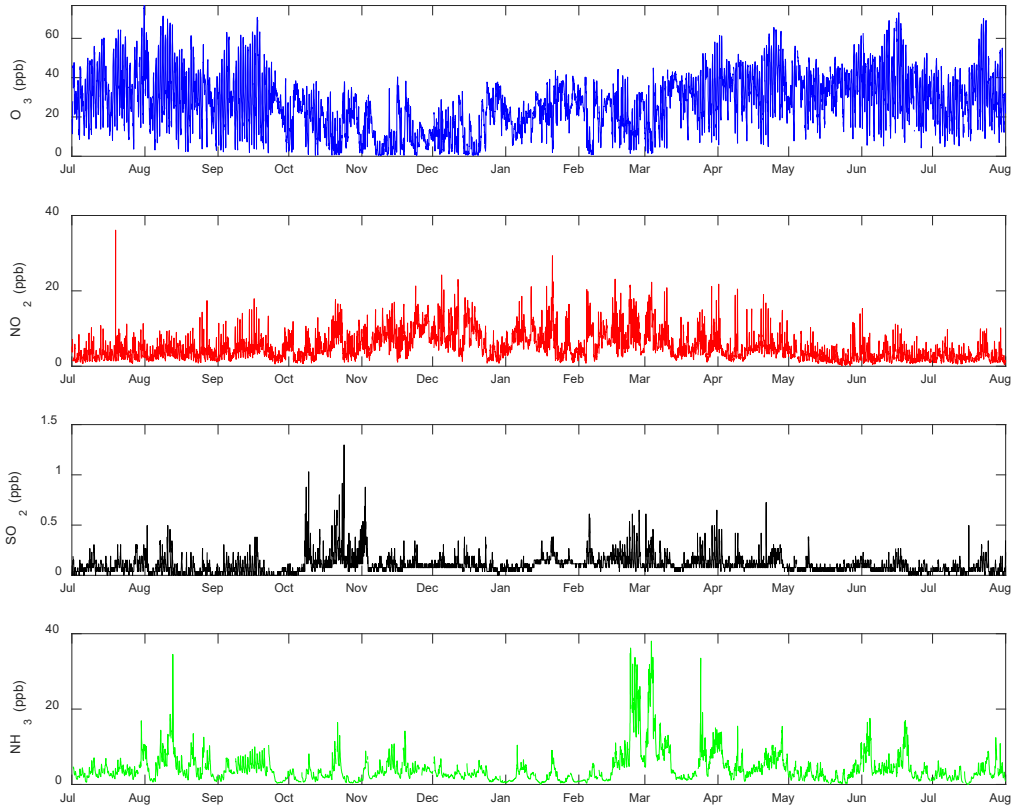

Figure S 7 Time series (hourly data) of trace gases in Payerne during our measurement period July 2020 – July 2021, Tick labels refer to the beginning of every month.

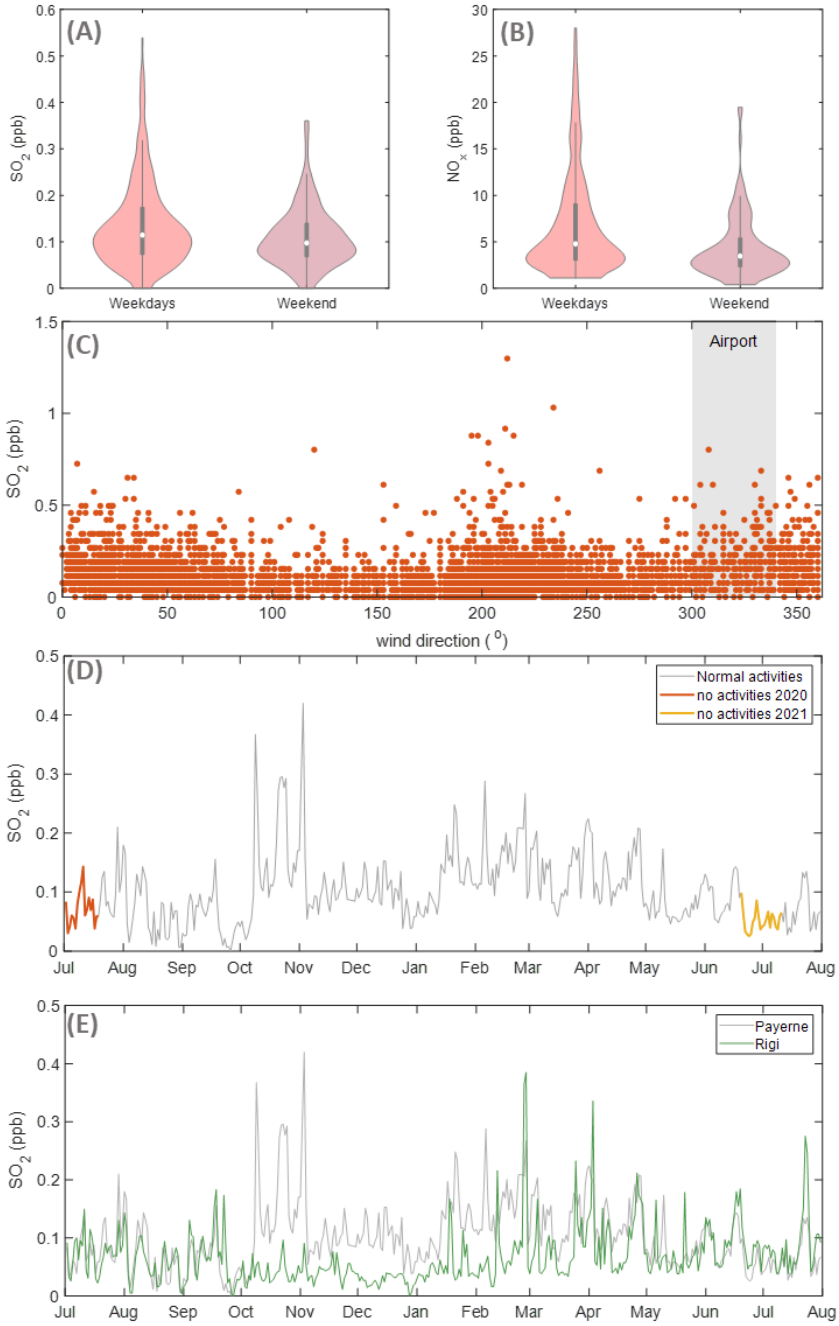

Figure S 8 Influence of airport activities on trace gases concentrations. (A) violin plot showing the concentration of SO_2 during airport working hours (8:00 – 17:00 CET), (B) violin plot showing the concentration of NO_x during airport working hours (8:00 – 17:00 CET), (C) SO_2 concentration (hourly averages) as a function of wind direction, wind direction from the airport is shaded. (D) time series of SO_2 concentration (daily averages) during normal activities and airport holidays. (DE) time series of SO_2 concentration (daily averages) in Payerne and Rigi- Seebodenalp (185 km away from Payerne and at an altitude of 1031 m a.s.l.). The difference in the SO_2 concentrations during winter and spring could be attributed to the shallower boundary layer height trapping the SO_2 at lower altitudes.

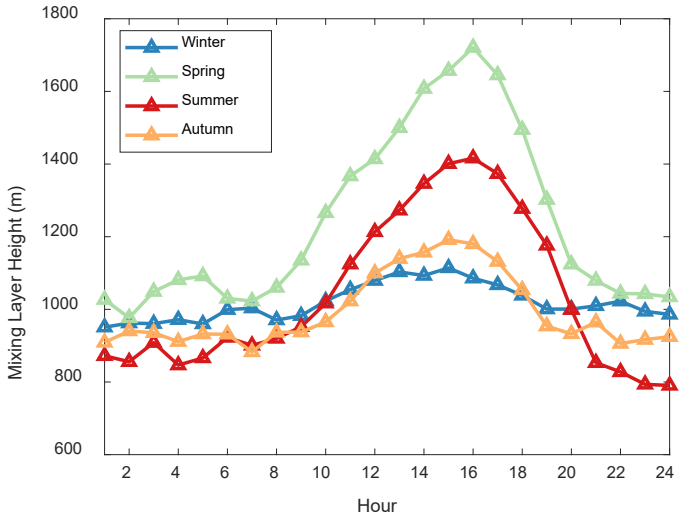

Figure S 9 Mixing layer height (MLH) estimated by the bulk Richardson method (Collaud Coen et al., 2014).

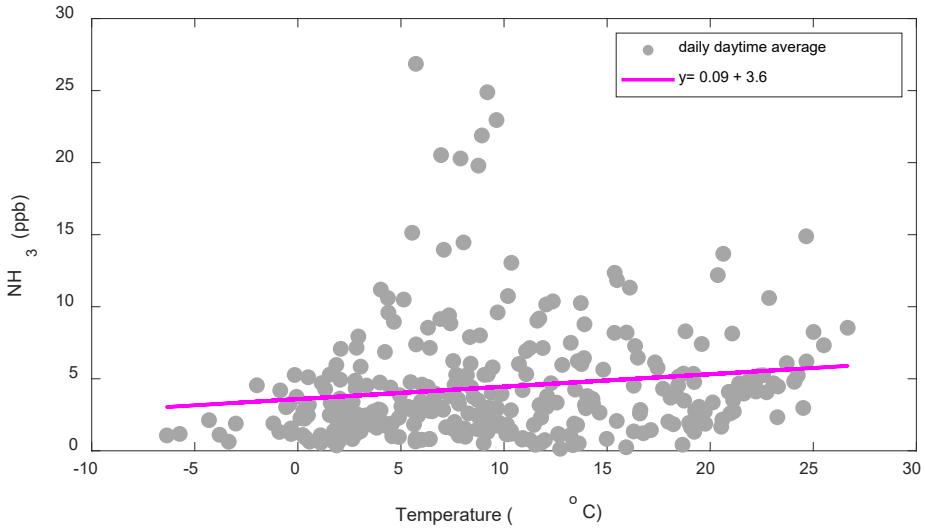

Figure S 10 Daily daytime (8:00 – 17:00 CEST, i.e., UTC+1) averages of NH_3 gas mixing ratio as a function of temperature.

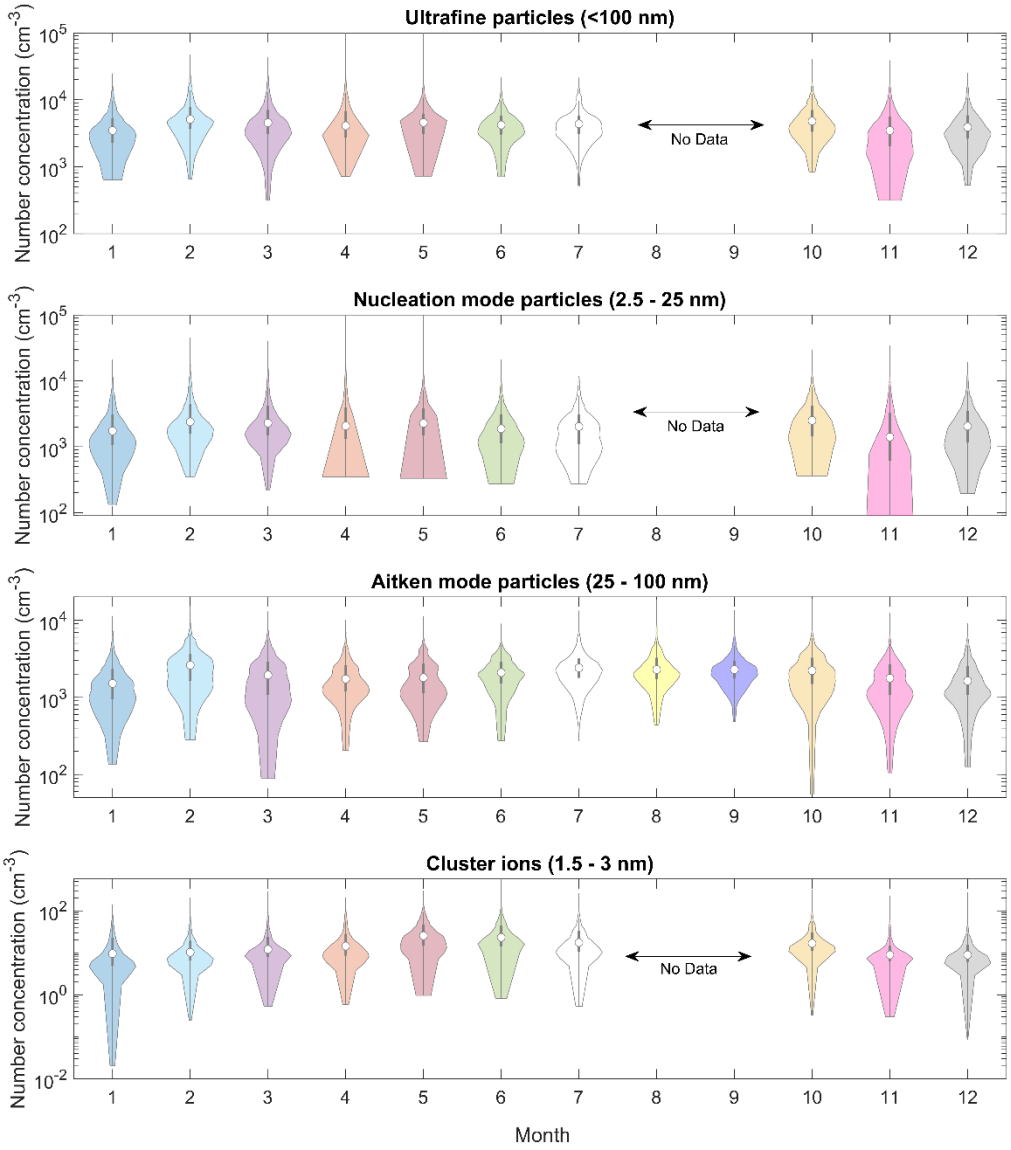

Figure S 11 Seasonality number concentration distributions of ultrafine, nucleation mode and Aitken mode particles and cluster ions (positive) in Payerne. No data from August and September is available for the ultrafine and nucleation mode particles and cluster ions. For the Aitken mode particles, July includes 2020 and 2021 concentrations. Data included in ultrafine, nucleation mode and cluster mode concentrations are in 5 min time steps (NAIS time stamp), while the Aitken mode concentrations are in 3 min time steps (SMPS time stamp).

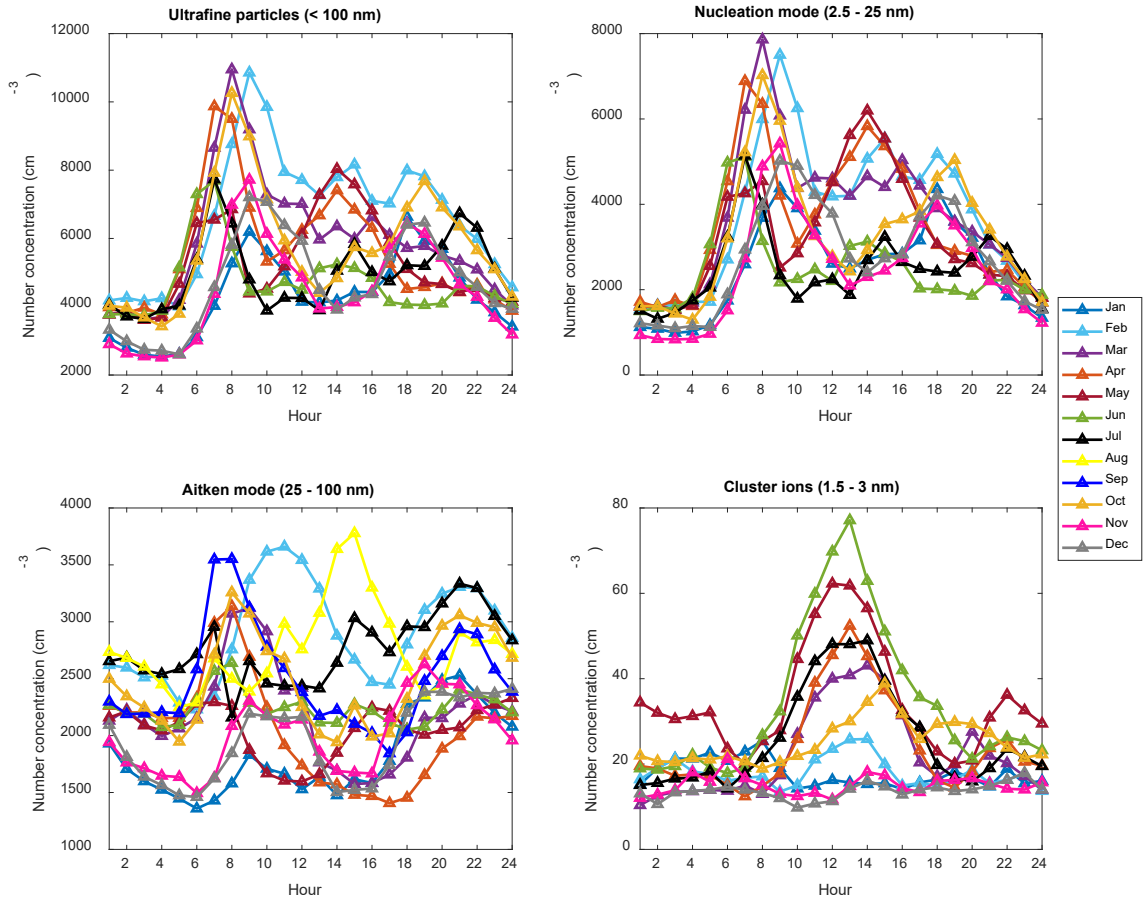

Figure S 12 Monthly diurnal concentrations of ultrafine, nucleation mode, Aitken mode particles and cluster ions (positive) in Payerne. No data from August and September is available for the ultrafine and nucleation mode particles or cluster ions. For the Aitken mode particles, July includes 2020 and 2021 concentrations. Data included in ultrafine, nucleation mode and cluster ion mode concentrations are in 5 min time steps (NAIS time stamp), while the Aitken mode concentrations are in 3 min time steps (SMPS time stamp).

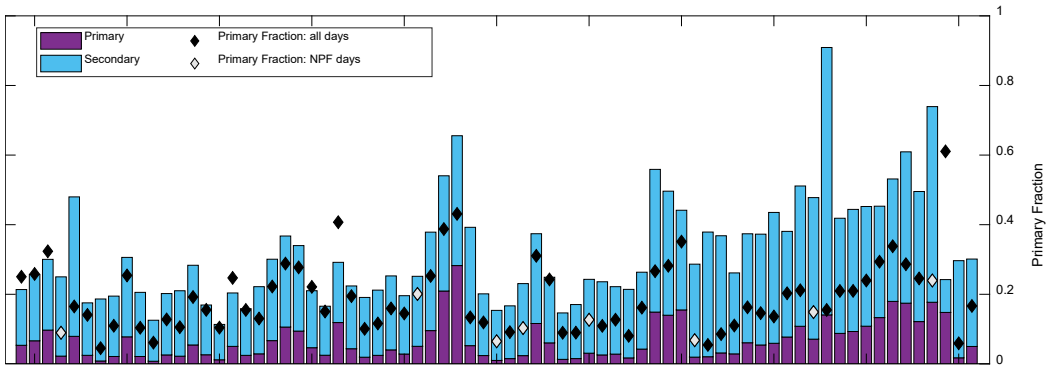

Figure S 13 Non-volatiles method: Average non-volatile (primary) and secondary ultrafine particles (<100 nm) shown as bar plot. The right axis shows the fraction of primary fraction as diamonds with hollow markers indicating NPF event days.

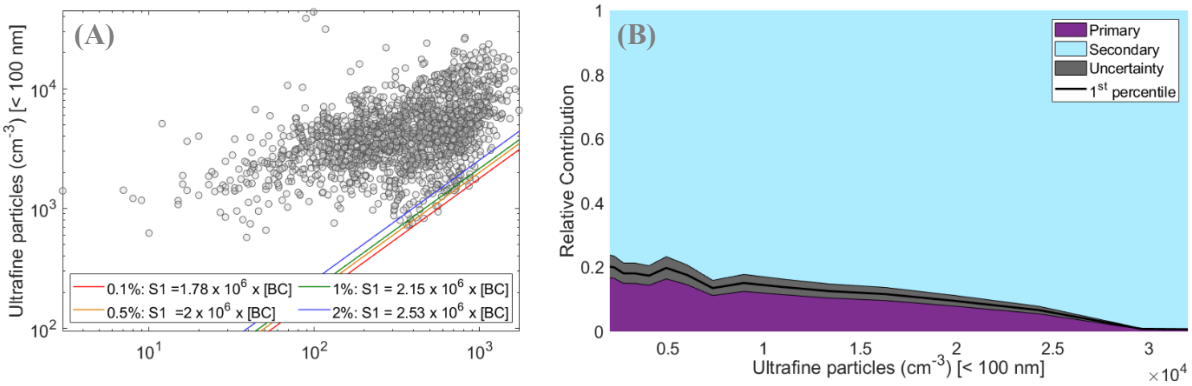

Figure S 14 BC tracer method (A) Ultrafine particle number concentration as a function of BC. The solid lines represent specific percentiles of the UFP number to BC mass ratio distribution, i.e. the specified fraction of data points falls below these lines. For example, the first percentile corresponds to 2.15 (x10^6) cm^{-3} primary particles per 1 ng/m^3 of BC are observed. (B) Relative contribution of primary and secondary ultrafine particles at different concentrations obtained from binned constrained fits from the different percentiles of N to BC ratio in Fig. S14 A. The uncertainty range indicates sensitivity of the BC tracer method to choosing the percentile between 0.1% and 2%.

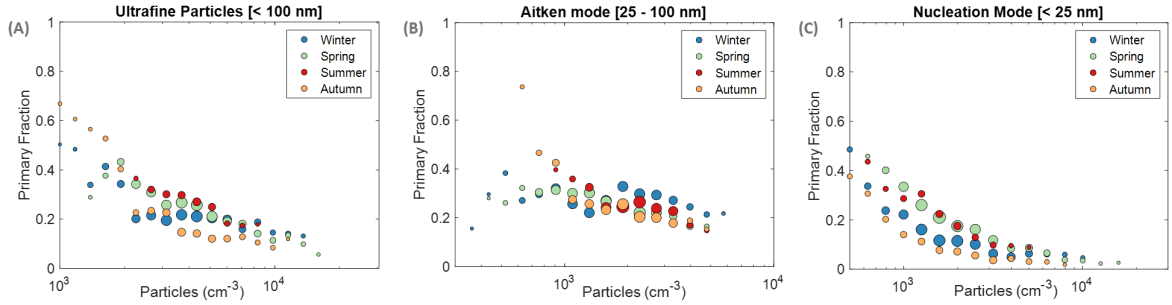

Figure S 15 Fraction of primary particles in the (A) ultrafine, (B) Aitken and (C) nucleation modes using the BC tracer method displayed as a function of their relative particle concentration. Each point is the median binned data to the particle concentration on the x-axis, with the size indicating the number of data points within each bin. Only bins which include more than 1% of the total data points are retained.

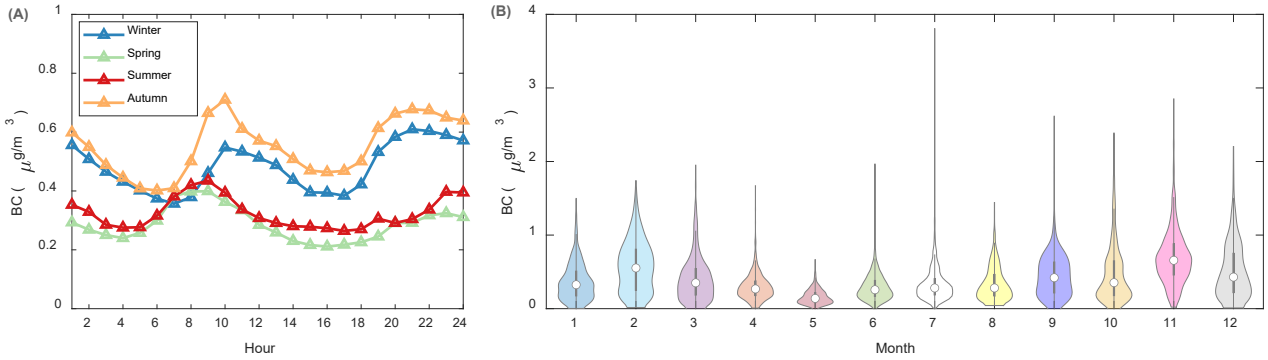

Figure S 16 (A) Seasonal diurnal average and (B) monthly variation of BC (880 nm) mass concentrations. Data include 13 months, 2020 and 2021 concentrations.

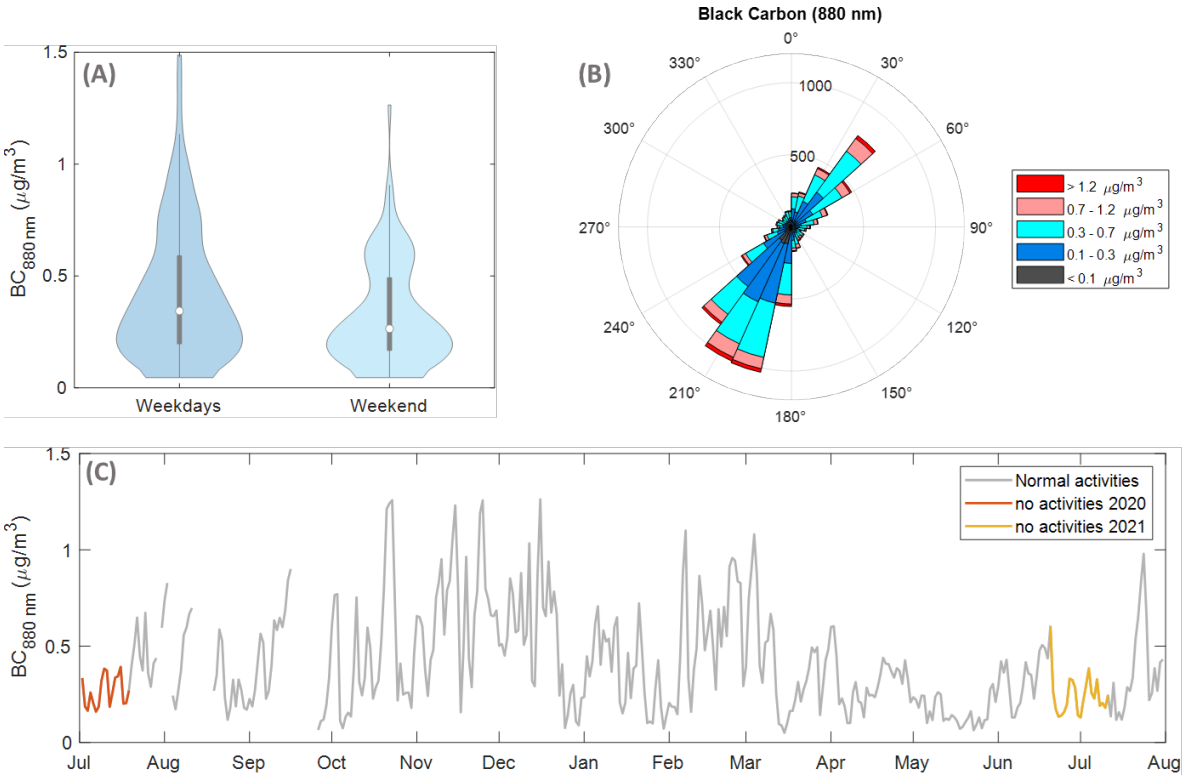

Figure S 17 Influence of airport activities on BC concentrations at 880 nm wavelength. (A) violin plot showing the concentration of BC during airport working hours (8:00 – 17:00 CET) on weekdays and weekends, (B) wind roses (30 bins) showing BC concentrations from different wind directions - airport direction (NW: 300 – 340°) (C) time series of BC concentration (daily averages) during normal activities and airport holidays. Tick labels refer to the beginning of every month.

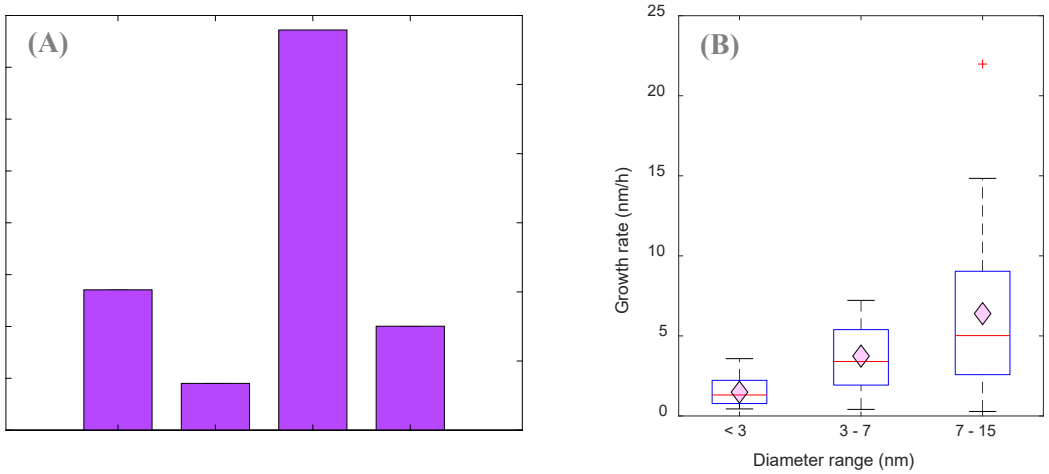

Figure S 18 (A) Frequency of different classes of events in Payerne. (B) Boxplots of the growth rates of particles in the size ranges sub-3, 3- 7 nm and 7 – 15 nm, calculated using the 50% appearance time method from the NAIS positive ions. The pink diamonds are the mean value of the distribution. The red line represents the median of the data included in each box and the lower and upper edges of the box represent 25th and 75th percentiles of the data, respectively. The length of the whiskers represents 1.5× interquartile range which includes 99.3 % of the data. Data outside the whiskers are considered outliers and are marked with red crosses.

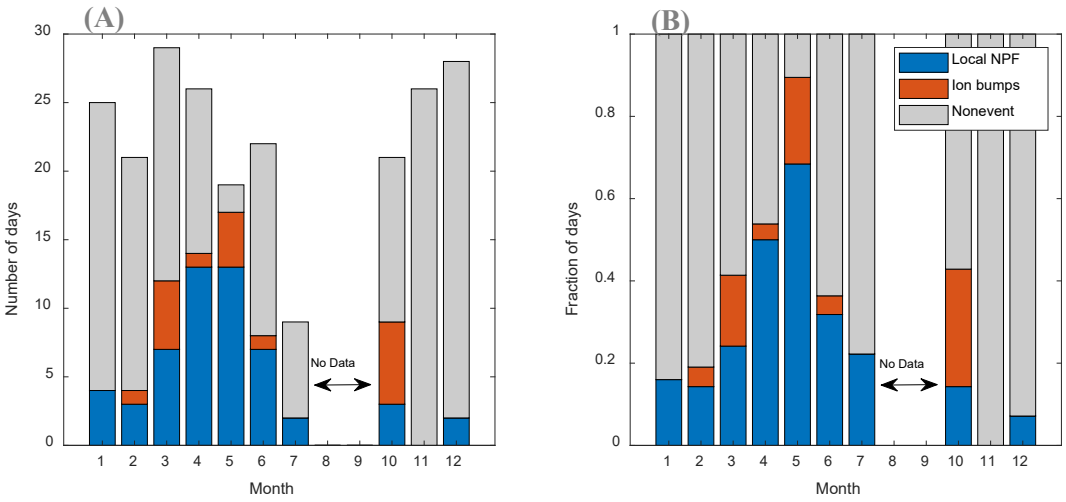

Figure S 19 Monthly (A) frequency and (B) fraction of different event classes in Payerne.

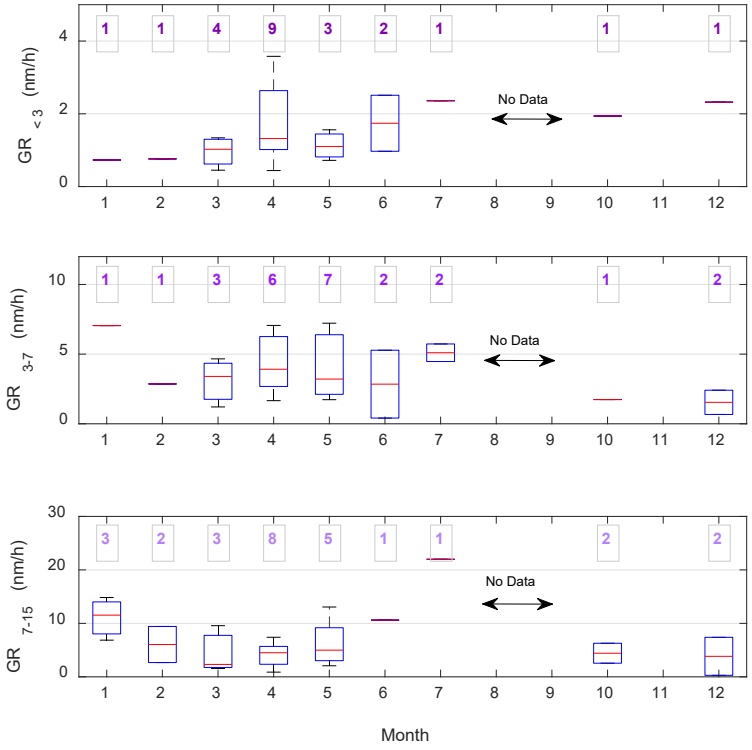

Figure S 20 Boxplots of the monthly growth rates of particles in the size ranges sub-3, 3- 7 nm and 7 – 15 nm, calculated using the 50% appearance time method from the NAIS positive ions. The number above each of the boxes in purple is the number of data points included in the box. The red line represents the median of the data included in each box and the lower and upper edges of the box represent 25th and 75th percentiles of the data, respectively. The length of the whiskers represent 1.5× interquartile range which includes 99.3 % of the data. No UFP data in the size range < 10 nm is available in August and September, while no event days are observed in November.

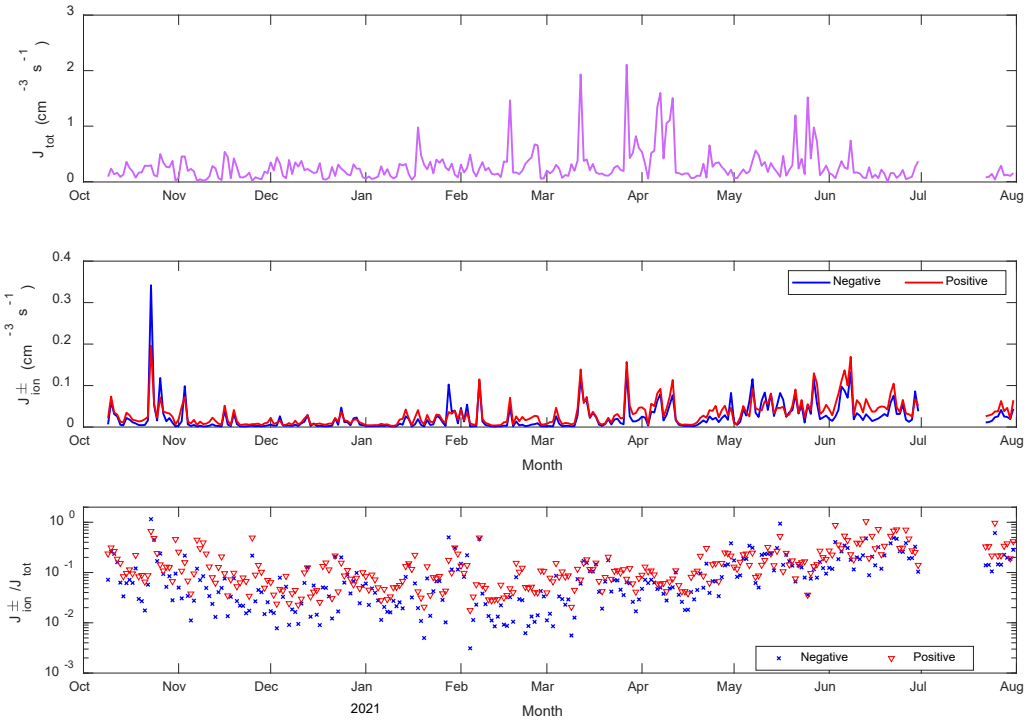

115

Figure S 21 Time series of particle formation rates of 2.5 nm particles and 1.5 nm negative and positive ions and ratio between ion and total formation rates. Data include daily daytime (8:00 – 17:00 LT) averages.

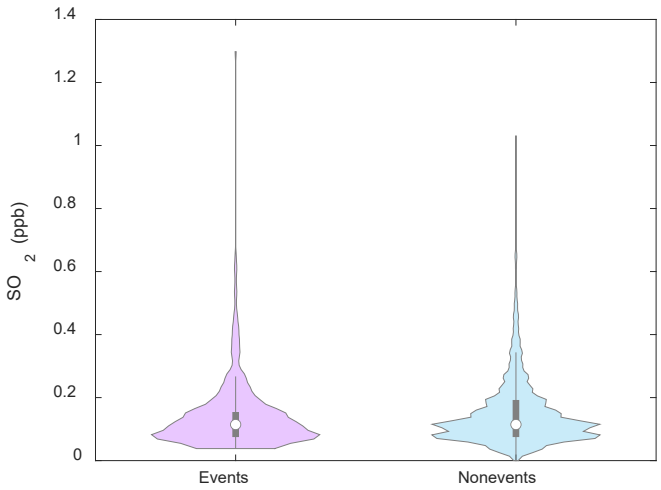

120 **Figure S 22 SO_2 concentrations on event (pink) and non-event days (blue) shown as violin plots. Violin plots are a combination of boxplot and a kernel distribution function on each side of the boxplots. The white circles define the median of the distribution and the edges on the inner grey boxes refer to the 25th and 75th percentiles, respectively.**

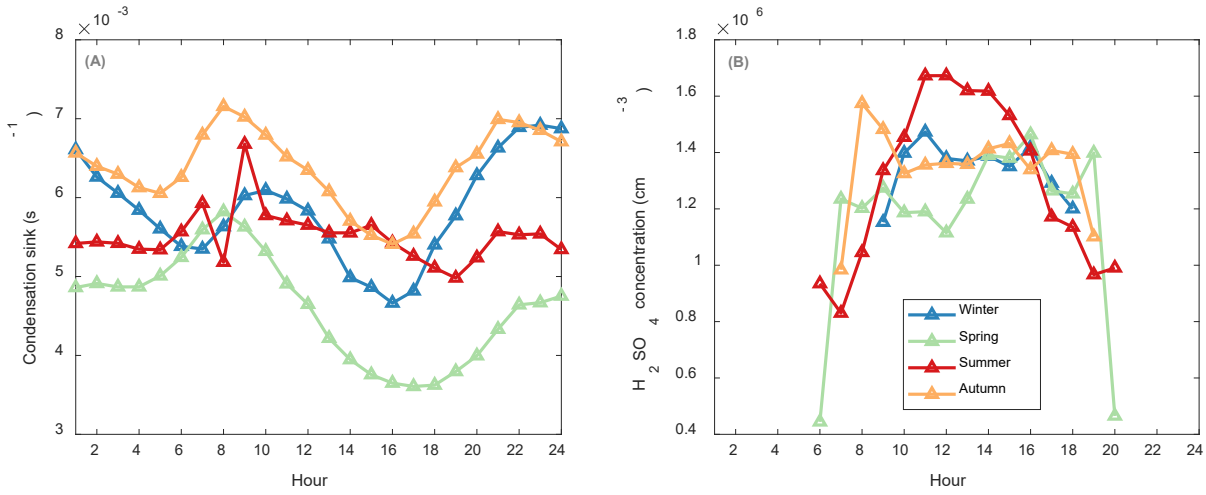

Figure S 23 Seasonal diurnal averages of (A) condensation sink and (B) H_2SO_4 proxy concentrations in Payerne.

125

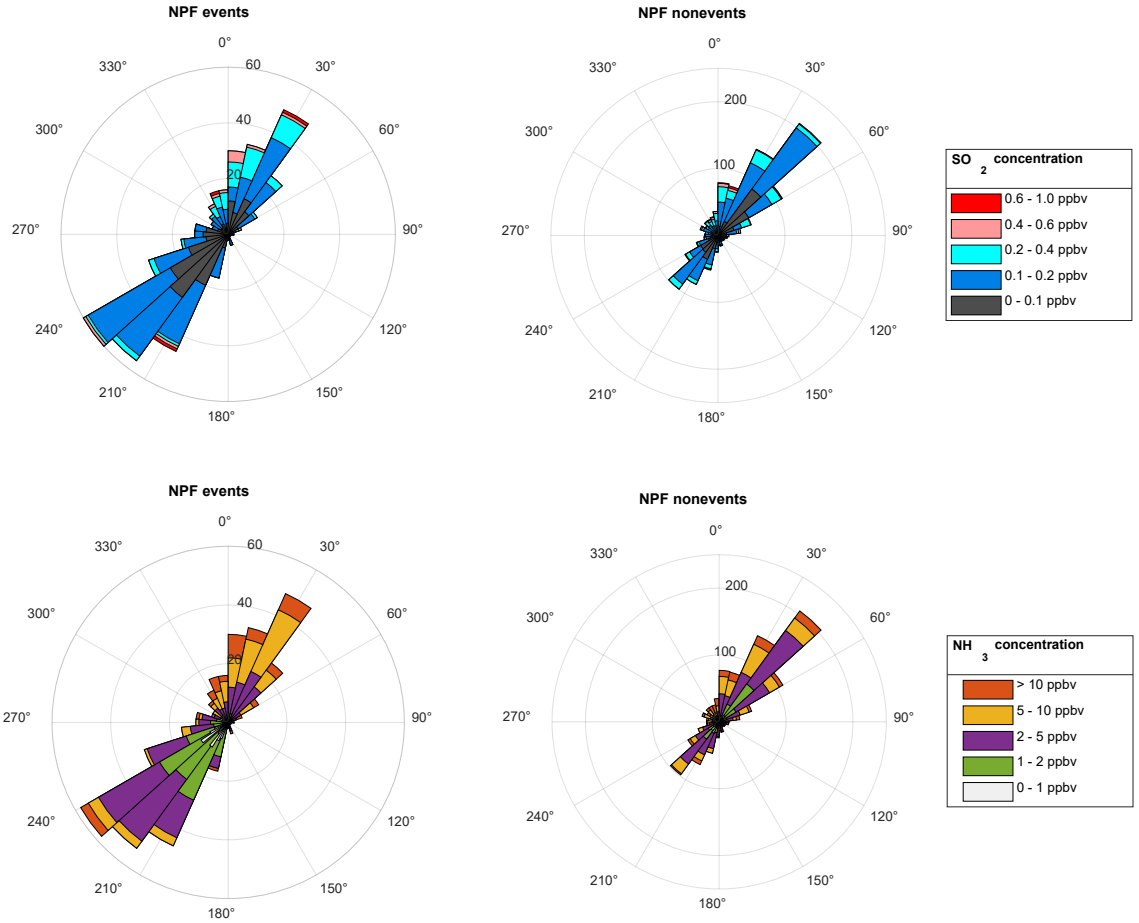

Figure S 24 Wind roses of SO_2 and NH_3 trace gas concentrations on NPF event and nonevent days divided into 30 bins.

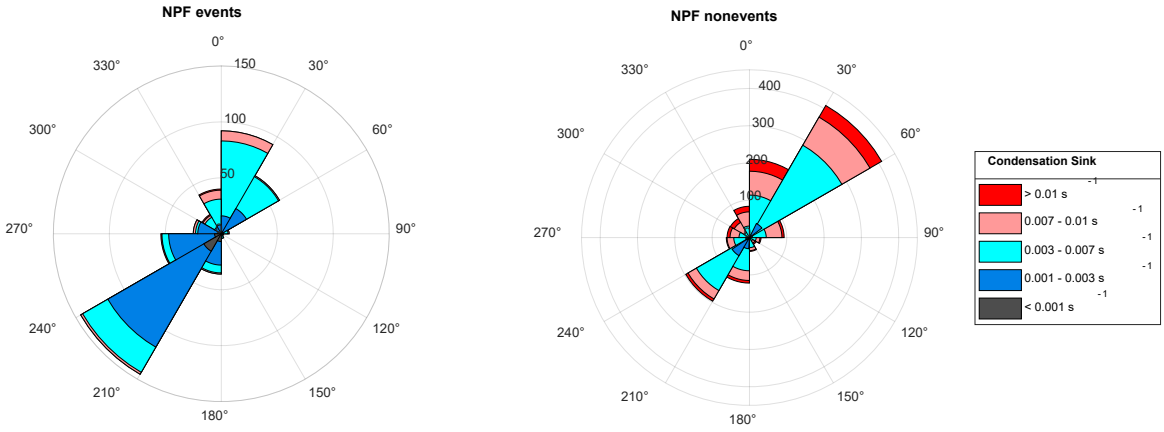

130 **Figure S 25 Wind roses of condensation sink on NPF event and nonevent days, divided into 12 bins.**

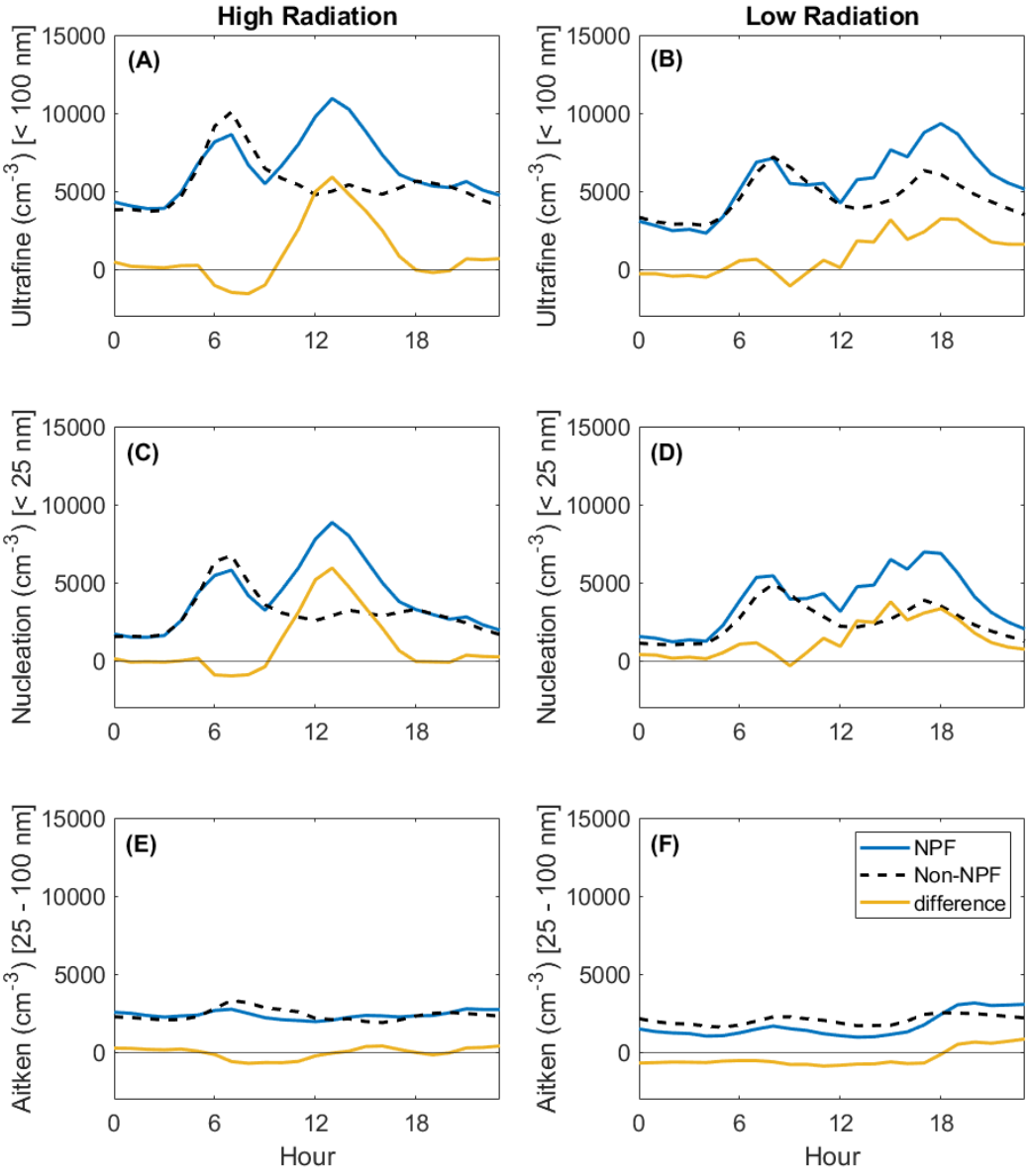

135 **Figure S 26 Diurnal average concentrations of (A) Ultrafine particles on NPF event, nonevent days and their difference during high radiation days (GlobRad ≥ 100 Wm^{-2}), and (B) during low radiation days (GlobRad < 100 Wm^{-2}), (C) Nucleation mode particles on NPF event, nonevent days and their difference during high radiation days, and (D) during low radiation days, and (E) Aitken mode particles on NPF event, nonevent days and their difference during high radiation days, and (F) during low radiation days.**

140 References

Collaud Coen, M., Praz, C., Haefele, A., Ruffieux, D., Kaufmann, P., and Calpini, B.: Determination and climatology of the planetary boundary layer height above the Swiss plateau by in situ and remote sensing measurements as well as by the COSMO-2 model, Atmos. Chem. Phys., 14, 13205-13221, 10.5194/acp-14-
145 13205-2014, 2014.

Dada, L., Chellapermal, R., Buenrostro Mazon, S., Paasonen, P., Lampilahti, J., Manninen, H. E., Junninen, H., Petäjä, T., Kerminen, V. M., and Kulmala, M.: Refined classification and characterization of atmospheric new-particle formation events using air ions, Atmos. Chem. Phys., 18, 17883-17893, 10.5194/acp-18-17883-2018, 2018.

150 Kerminen, V.-M. and Kulmala, M.: Analytical formulae connecting the “real” and the “apparent” nucleation rate and the nuclei number concentration for atmospheric nucleation events, Journal of Aerosol Science, 33, 609-622, 10.1016/S0021-8502(01)00194-X, 2002.